

## Supporting Information

### Porous NiCoP Nanosheet as Efficient and Stable Positive Electrode for Advanced Asymmetric Supercapacitors

Xiaomeng Zhang, Aiping Wu, Xiuwen Wang, Chungui Tian,\* Ruiyue An and Honggang Fu\*

#### The content of ESI

**Figure S1.** XRD patterns of (a) NiCo-precursor and S-NiCoP-2-300, (b) S-NiCoP-2-250and S-NiCoP-2-350.

**Figure S2.** XPS full profiles for NiP-300 and CoP-300.

**Figure S3.** High-resolution XPS spectra of NiP-300 for (a) Ni 2p and(b) P 2p; CoP-300 for (c) Co 2p, (d) P 2p.

**Figure S4.** Nitrogen adsorption–desorption isotherm and pore size distribution (inset) of (a) S-NiCoP-1-300, (b) S-NiCoP-3-300, (c) S-NiCoP-2-250 and (d) S-NiCoP-2-350.

**Figure S5.** Specific capacitances of the S-NiCoP-2-300 coated Ni foam electrodes as a function of the mass loading of S-NiCoP-2-300 sample (from 0.32 to 13.5 mg cm<sup>-2</sup>).

**Figure S6.** Electrochemical performance of S-NiCoP-1-300, S-NiCoP-3-300, S-NiCoP-2-250 and S-NiCoP-2-350 for supercapacitors:(a) CV curves at different scan rate of 10 mV s<sup>-1</sup>; (b) Galvanostatic charge/discharge curves at a current density of 1 A g<sup>-1</sup>.

**Figure S7.** The specific capacitances of the as-prepared samples at different current densities.

**Table S1.** The experimental parameters of the different samples. The HT represented hydrothermal temperature, and PT is phosphorization temperature.

**Table S2.** Textual parameters of the Ni-Co-based materials, NiP-300 and CoP-300.

**Table S3.** The discharge specific capacitance at different current densities for samples.

**Table S4.** The capacitance performance of representative TMPs.

**Table S5.** Comparison of area capacitances with the published materials.

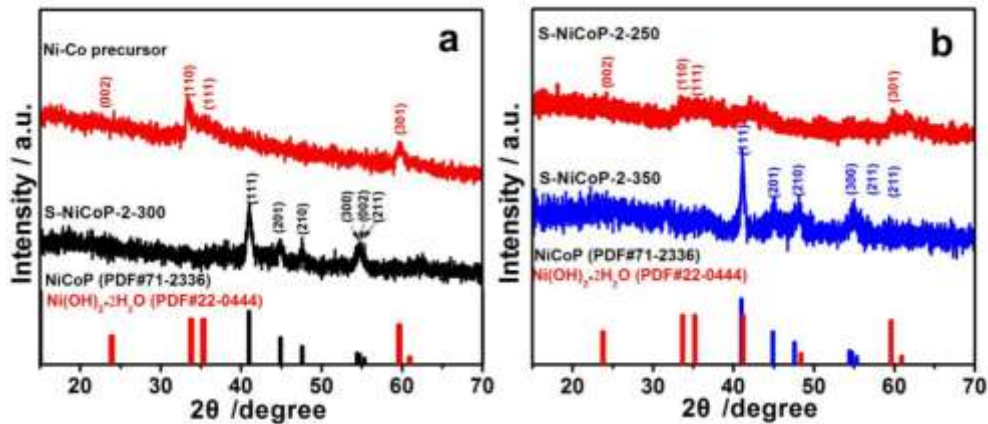


**Figure S1.** XRD patterns of (a) NiCo-precursor and S-NiCoP-2-300, (b) S-NiCoP-2-250and S-NiCoP-2-350.

The peaks located at  $33.6^\circ$ ,  $35.2^\circ$  and  $60.9^\circ$  can be indexed to (110) (111) and (301) planes of NiCo-precursor (JCPDS no. 22-0444) (Figure S1a). The new diffraction peaks emerge upon phosphorization, which match well with the hexagonal NiCoP (JCPDS no.71-2336). The sharp diffraction peaks located at  $41.0^\circ$ ,  $44.9^\circ$ ,  $47.6^\circ$ ,  $54.4^\circ$ ,  $54.7^\circ$  and  $55.3^\circ$ can be assigned to (111) (201), (210), (300), (002), and (211) plane of hexagonal NiCoP, respectively. For comparison, the phosphating temperatures have been tuned to  $250^\circ\text{C}$  (S-NiCoP-2-250) and  $350^\circ\text{C}$  (S-NiCoP-2-350) (Figure S1b). The XRD of S-NiCoP-2-250 have shown similar pattern with that of NiCo-precursor, indicating that the low temperature is not favourable for the conversion reaction. In contrast, the S-NiCoP-2-350 gives a XRD pattern well-matched to NiCoP (JCPDS no. 71-2336).

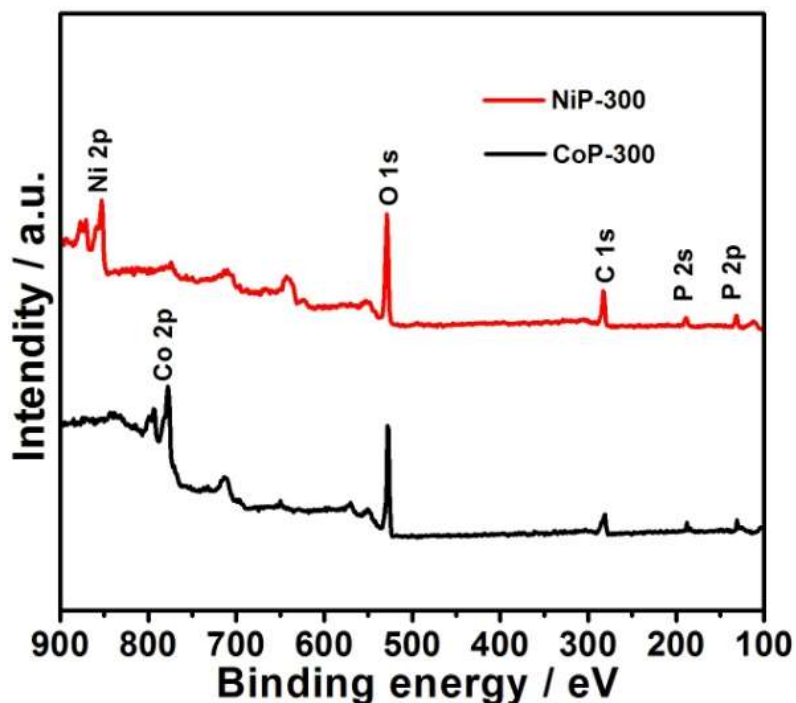


**Figure S2.** XPS full profiles for NiP-300 and CoP-300.

Figure S2 shows XPS full profiles for NiP-300 and CoP-300. The XPS full survey spectra of NiP-300 show the existence of Ni, P, C and O peaks. For CoP-300, the Co, P, C and O peaks can be obviously seen. The results imply the formation of NiP and CoP.

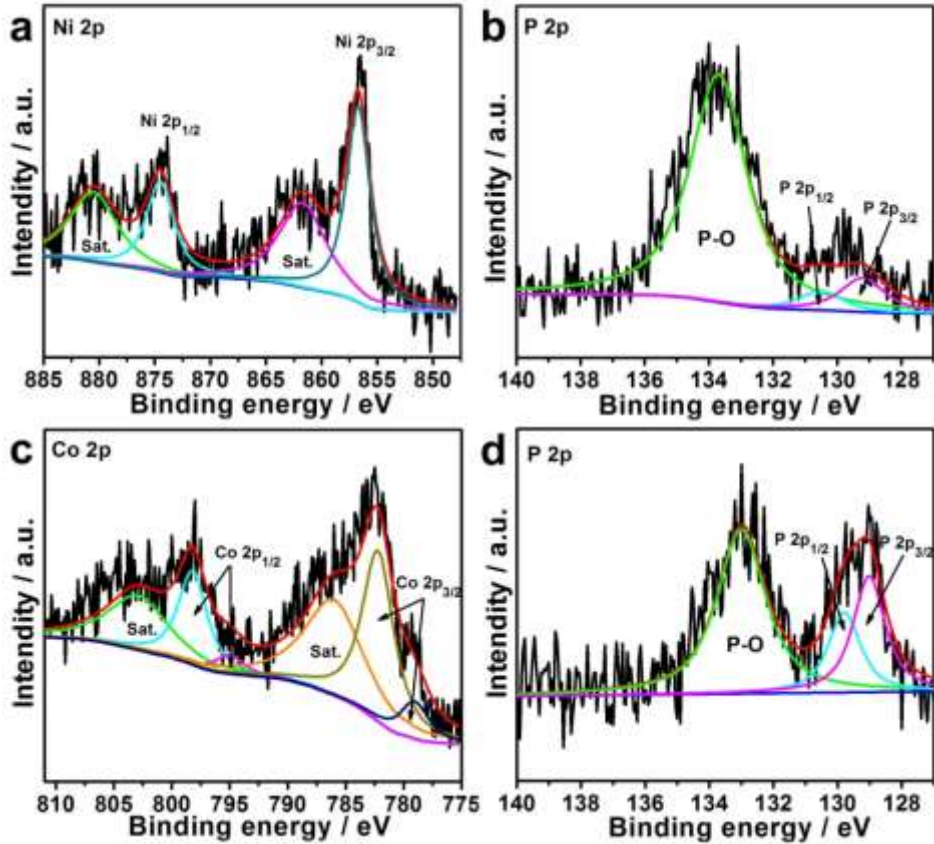


**Figure S3.** High-resolution XPS spectra of NiP-300 for (a) Ni 2p and (b) P 2p; CoP-300 for (c) Co 2p, (d) P 2p.

Figure S3 shows high-resolution individual XPS spectra of for NiP-300 and CoP-300. The Ni 2p spectrum can be fitted with two spin-orbit doublets and two shake-up satellites (marked Sat.). In P 2p spectrum (Figure S 3b), the peaks located at about 129.7 and 128.9 eV are close to binding energy of P 2p 1/2 and P 2p 3/2 of P in metal phosphide. The broad peak at 132.9 eV is typical of phosphate species, likely due to superficial passivation of metal phosphide. Figure S 3c plot the high-resolution XPS spectra of CoP-300 in the Co 2p regions. As we can see two typical peaks are ascribed to Co 2p<sub>3/2</sub> and Co 2p<sub>1/2</sub> of Co species in the phosphide, respectively, along with two apparent satellite peaks. In the Figure S 3d, the peak centered at 130.5 eV and 129.2 eV may be

assigned to P 2p 1/2 and P 2p 3/2, respectively. The broad peak at 133.6 eV is typical of phosphate species.

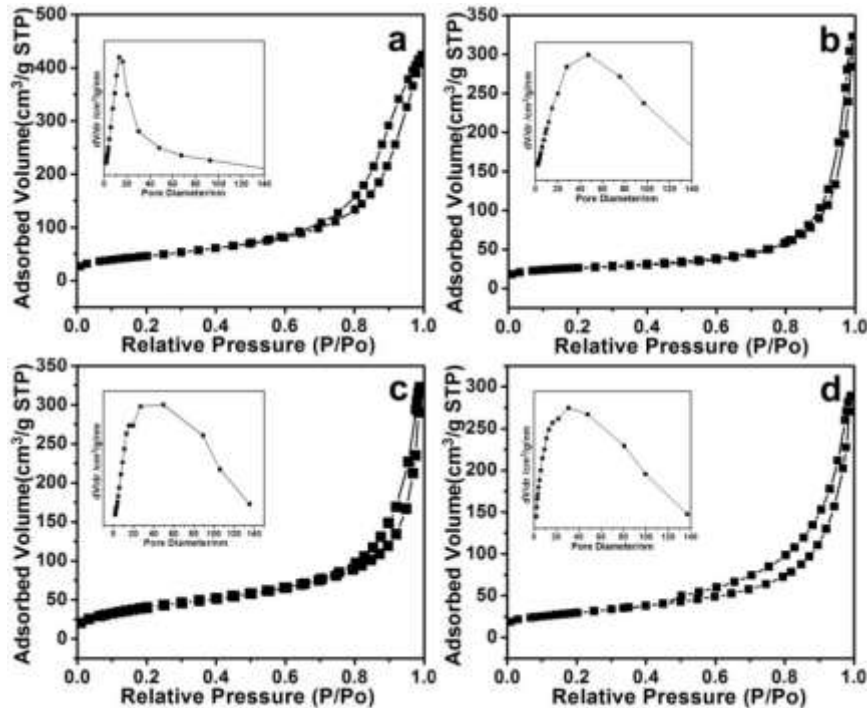


**Figure S4.** Nitrogen adsorption–desorption isotherm and pore size distribution (inset) of (a) S-NiCoP-1-300, (b) S-NiCoP-3-300, (c) S-NiCoP-2-250 and (d) S-NiCoP-2-350.

The experimental parameters have large influence on the  $S_{\text{BET}}$  of final phosphating product. The  $N_2$  isothermal adsorption-desorption test results of S-NiCoP-2-250 are very close to that of Ni-Co precursor ( $S_{\text{BET}}: 147.91 \text{ m}^2\text{g}^{-1}$ ). The similarity should be contributed the less transformation of precursor to phosphide at relative low temperature. As the temperature rises further, the sample (S-NiCoP-2-350) have shown a low specific surface area of  $91.65 \text{ m}^2\text{g}^{-1}$ . The relative low values should

be due to the growth of nanoparticles and aggregation of nano-sheets under high phosphating temperature. The S-NiCoP-2-300 have shown the high  $S_{BET}$  due the proper calcination temperature can make the transformation of precursor into NiCoP, the formation of the pores with a avoidance of the excessive growth of nanoparticles and aggregation of nano-sheets.

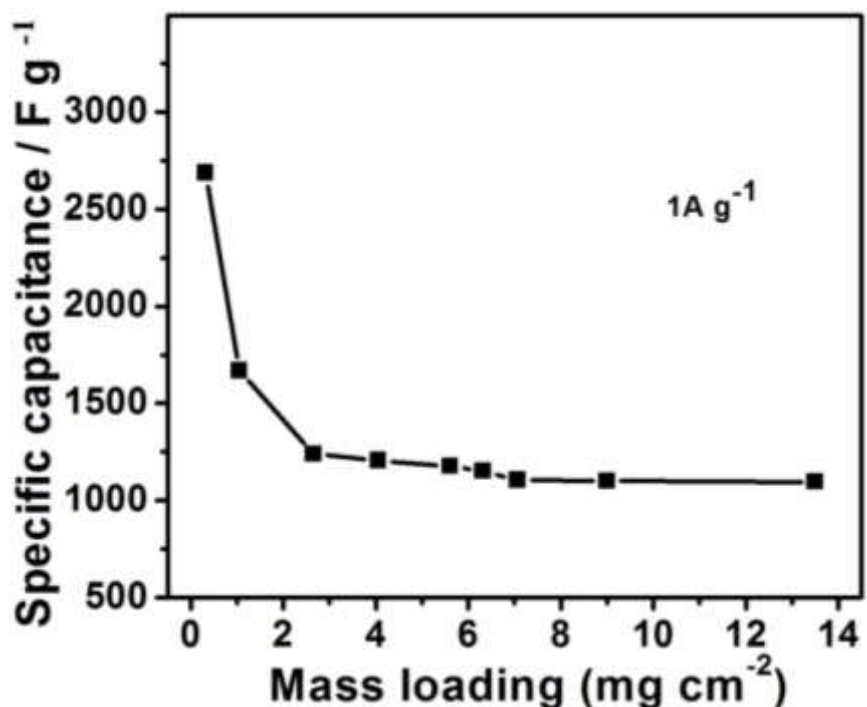


**Figure S5.** Specific capacitances of the S-NiCoP-2-300 coated Ni foam electrodes as a function of the mass loading of S-NiCoP-2-300 sample (from  $0.32$  to  $13.5 \text{ mg cm}^{-2}$ ).

The mass loading of S-NiCoP-2-300 on Ni foam are changed from  $0.32$  to  $13.5 \text{ mg cm}^{-2}$  to study the effect (Figure S5). We can see that the high capacitance can be obtained in the case of low mass loading ( $2687 \text{ Fg}^{-1}$ ). However, too little coating mass of active components are not real for practical application. The specific mass

capacitance gradually decreased with the increase mass loading until the mass reached to  $2.65 \text{ mg cm}^{-2}$ . Further increase mass loading can not induce obvious change of capacitance value. For example, the value is about  $1240 \text{ F g}^{-1}$  and  $1095 \text{ F g}^{-1}$  for the loading mass of  $2.65 \text{ mg cm}^{-2}$  and  $13.5 \text{ mg cm}^{-2}$ . Notably, even at high loading mass of  $13.5 \text{ mg cm}^{-2}$ , the electrode still exhibit a high discharge specific capacitances of  $1095 \text{ F g}^{-1}$ , being similar to that of  $4 \text{ mg cm}^{-2}$ . The excellent capacitance behavior is intimately related with the ability of effective transmission of ions by the porous structure, but also benefits from the rapid transfer of electrons by the TMPs structure.

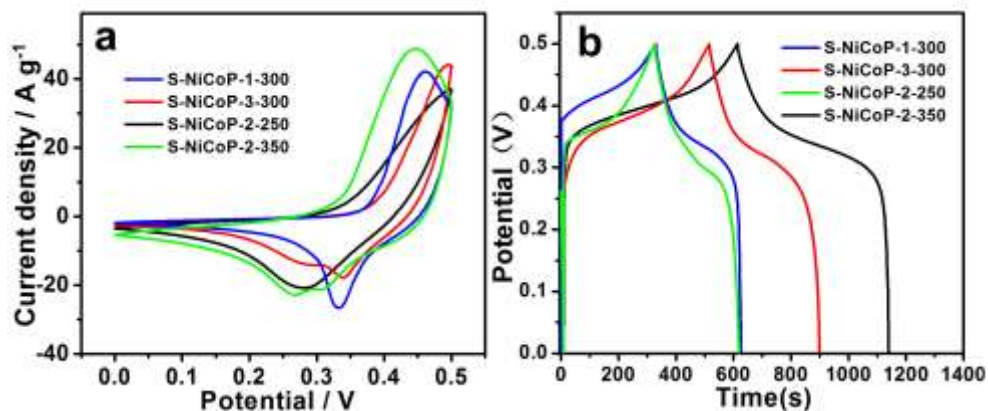


**Figure S6.** Electrochemical performance of S-NiCoP-1-300, S-NiCoP-3-300, S-NiCoP-2-250 and S-NiCoP-2-350 for supercapacitors:(a) CV curves at different scan rate of  $10 \text{ mV s}^{-1}$ ; (b) Galvanostatic charge/discharge curves at a current density of  $1 \text{ A g}^{-1}$ .

CV curves of NiCo-based samples at a constant scan rate of  $10 \text{ mV s}^{-1}$  are shown in Figure S5a. All the NiCo-based samples exhibit an larger CV curve area in comparison to NiCo-precursor, indicating an increased area specific capability of NiCo-based phosphides. The enhancement can well be correlated to the lower electronegativity of P in metal phosphides (that facilitates redox reactions) and the

increased reactive surface area arising from the porous structure with high specific surface areas. The capacitance are about  $609 \text{ F g}^{-1}$ ,  $816 \text{ F g}^{-1}$ ,  $581 \text{ F g}^{-1}$  and  $1049 \text{ F g}^{-1}$  for S-NiCoP-1-300, S-NiCoP-3-300, S-NiCoP-2-250, S-NiCoP-2-350, respectively. All the NiCo-based phosphides much higher than those for Ni-Co precursor ( $566 \text{ F g}^{-1}$ ), CoP-300 ( $404 \text{ F g}^{-1}$ ) and NiP-300 ( $436 \text{ F g}^{-1}$ ). The improved performance of NiCo-based phosphides demonstrates the superiority of the phosphide over that corresponding oxides, which should relative with the good conductivity of former than later, as well of specific structure of phosphide.

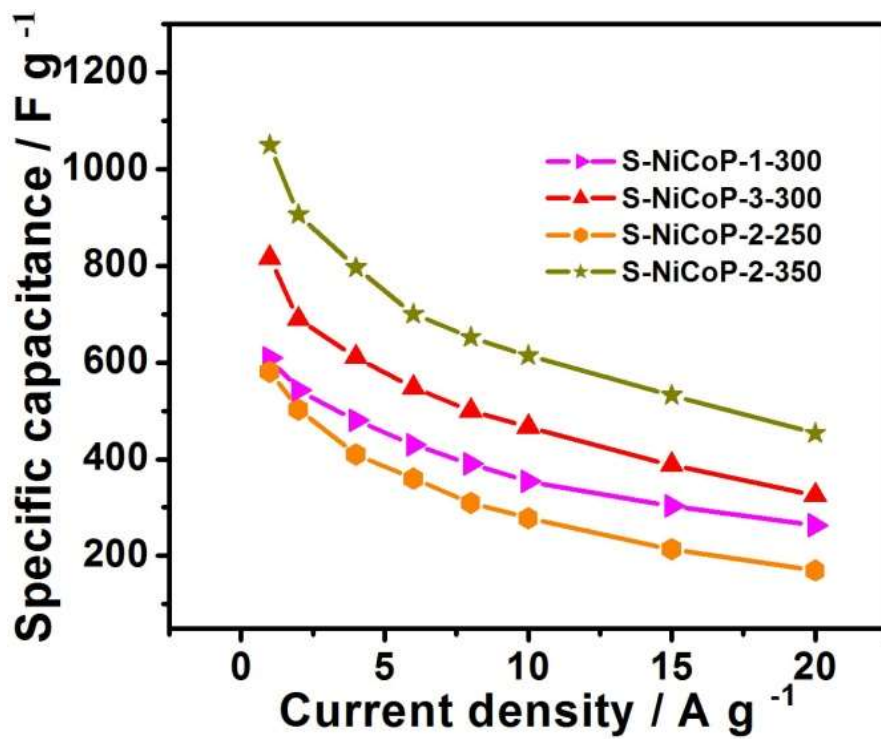


**Figure S7.** The specific capacitances of the as-prepared samples at different current densities.

**Table S1.** The experimental parameters of the different samples. The HT represented hydrothermal temperature, and PT is phosphorization temperature.

Sample	Ni(NO <sub>3</sub> ) <sub>2</sub> (mmol)	Co(NO <sub>3</sub> ) <sub>2</sub> (mmol)	HT (°C)	PT (°C)
<b>Ni-Co precursor</b>	15	15	200	300°C
S-NiCoP-1-300	10	20	200	300°C
S-NiCoP-2-300	15	15	200	300°C
S-NiCoP-3-300	20	10	200	300°C
CoP-300	0	30	200	300°C
NiP-300	30	0	200	300°C
S-NiCoP-1-250	15	15	200	250°C
S-NiCoP-1-350	15	15	200	350°C

**Table S2.** Textual parameters of the Ni-Co-based materials, NiP-300 and CoP-300.

samples	S <sub>BET</sub> (m <sup>2</sup> g <sup>-1</sup> )	Pore volume (cm <sup>3</sup> g <sup>-1</sup> )	Pore size (nm)
<b>Ni-Co precursor</b>	147.9	0.46	16.41
S-NiCoP-1-300	163.3	0.55	11.74
S-NiCoP-2-300	216.4	0.62	12.07
S-NiCoP-3-300	91.7	0.44	21.37
CoP-300	55.4	0.17	14.64
NiP-300	88.1	0.12	8.49
S-NiCoP-2-250	148.0	0.41	15.98
S-NiCoP-2-350	104.3	0.38	15.48

**Table S3.** The discharge specific capacitance at different current densities for samples.

sample	C <sub>g</sub> (F/g)							
	1A/g	2A/g	4A/g	6A/g	8A/g	10A/g	15A/g	20A/g
NiCo-precursor	566	524	435	375	325	277	176	100
S-NiCoP-1-300	609	543	480	430	390	354	303	263
S-NiCoP-2-300	1206	1080	990	926	862	825	709	612
S-NiCoP-3-300	816	689	611	548	500	467	388	325
S-NiCoP-2-250	581	503	410	360	310	278	214	170
S-NiCoP-2-350	1049	906	796	700	652	614	532	454
NiP-300	436	380	319	267	236	206	147	101
CoP-300	404	377	349	327	308	298	270	244

**Table S4.** The capacitance performance of representative TMPs.

sample	Three-electrode			Two-electrode		ref.
	electrolyte	voltage	capacitance	E	P	
Ni <sub>2</sub> P/rGO nanoparticles	2 M KOH	0-0.5V	2266 Fg <sup>-1</sup> 5mA cm <sup>-2</sup>	-	-	1
Amorphous Ni-P	2 M KOH	0-0.4V	1338.75 F g <sup>-1</sup> 1Ag <sup>-1</sup>	29.2 Wh kg <sup>-1</sup>	400 W kg <sup>-1</sup>	2
Au/Ni <sub>12</sub> P <sub>5</sub> core/shell nanocrystals	2 M KOH	0-0.4V	571.4Fg <sup>-1</sup> 0.2A g <sup>-1</sup>	-	-	3
Co <sub>2</sub> P nanoflowers	6 M KOH	0-0.5V	416 Fg <sup>-1</sup> 1A g <sup>-1</sup>	8.8 Whkg <sup>-1</sup>	6kW kg <sup>-1</sup>	4
Ni <sub>2</sub> P particles	2 M KOH	0-0.4V	823.25 Fg <sup>-1</sup> 1A g <sup>-1</sup>	35.5 Whkg <sup>-1</sup>	400W kg <sup>-1</sup>	5
Ni <sub>2</sub> P <sub>4</sub> particles	2 M KOH	0-0.4V	801.5 Fg <sup>-1</sup> 1A g <sup>-1</sup>	29.8Whkg <sup>-1</sup>	400W kg <sup>-1</sup>	5
NiCoP particles	2 M KOH	0-0.4V	571Cg <sup>-1</sup> 1Ag <sup>-1</sup>	32Whkg <sup>-1</sup>	0.351kW kg <sup>-1</sup>	6
Ni <sub>2</sub> P/Ni <sub>12</sub> P <sub>5</sub> nanoparticles	2.0 M KOH	0-0.4V	147.3mAh g <sup>-1</sup> 1A g <sup>-1</sup>	32.1Wh kg <sup>-1</sup>	796.8W kg <sup>-1</sup>	7
Ni <sub>x</sub> Co <sub>1-x</sub> O/Ni <sub>y</sub> Co <sub>2-y</sub> P@C/Nickel Foam	6.0 M KOH	0-0.5V	2638 Fg <sup>-1</sup> 1A g <sup>-1</sup>	39.4Whkg <sup>-1</sup>	394W kg <sup>-1</sup>	8
Cu <sub>3</sub> P Nanotube Arrays	1 M H <sub>2</sub> SO <sub>4</sub>	0-0.5V	300 F g <sup>-1</sup> 2.5mAcm <sup>-2</sup>	-	17 kW kg <sup>-1</sup>	9
NiCoPnanoparticles	2.0 M KOH	0.1-0.58 V	646 Fg <sup>-1</sup> 4A g <sup>-1</sup>	-	-	10
NiCoPnanoplates/Carbon paper	1.0 M KOH	0-0.5V	194 mAh g <sup>-1</sup> 1 A g <sup>-1</sup>	32.9 Wh kg <sup>-1</sup>	1301 W kg <sup>-1</sup>	11
Ni <sub>12</sub> P <sub>5</sub> hollow nanocapsules	6M KOH	0-0.55V	949Fg <sup>-1</sup> 1A g <sup>-1</sup>	-	-	12
Ni <sub>2</sub> P nanorods	3M KOH	0- 0.475 V	799.2Fg <sup>-1</sup> 1A g <sup>-1</sup>	-	-	13
Ni-P microspheres@MnO <sub>2</sub>	6 M KOH + 0.7 M LiOH	0-0.35 V	1130Fg <sup>-1</sup> 1A g <sup>-1</sup>	10.9 Wh kg <sup>-1</sup>	5.6 kW kg <sup>-1</sup>	14
Mesoporous Ni-P@NiCo <sub>2</sub> O <sub>4</sub>	6 M KOH + 0.7 M LiOH	0-0.35 V	1240Fg <sup>-1</sup> 1A g <sup>-1</sup>	13.3 Wh kg <sup>-1</sup>	5.7 kW kg <sup>-1</sup>	15
NiCoP nanosheets	2 M KOH	0-0.5V	1206 Fg <sup>-1</sup> 1A g <sup>-1</sup>	36.32Wh kg <sup>-1</sup>	375 W kg <sup>-1</sup>	This work

**Table S5.** Comparison of area capacitances with the published materials.

sample	Three-electrode			ref.
	electrolyte	voltage	capacitance	
CoP nanowire/Carbon cloth	6.0 M KOH	0-0.4V	1.89 F/cm <sup>2</sup> (3mA/cm <sup>2</sup> )	16
NiCoP Nanoarray/Ni Foam	2.0 M KOH	0-0.5V	9.2 F cm <sup>-2</sup> 2 mA cm <sup>-2</sup> 5.97 F cm <sup>-2</sup> 50 mA cm <sup>-2</sup>	17
Co <sub>9</sub> S <sub>8</sub> /NiCo <sub>2</sub> S <sub>4</sub> nanosheet/Ni Foam	3.0 MKOH	0-0.5V	7.4F cm <sup>-2</sup> at 5mA cm <sup>-2</sup>	18
Ni-Co oxide /Ni Foam	2.0 MKOH	0-0.5V	11.44F cm <sup>-2</sup> at 1mA cm <sup>-2</sup>	19
urchin-like CoMn <sub>2</sub> O <sub>4</sub>	2.0 MKOH	0-0.5V	8.69F cm <sup>-2</sup> at 10 mA cm <sup>-2</sup>	20
Ni <sub>x</sub> Co <sub>1-x</sub> (OH) <sub>2</sub> nanosheet/carbon	1.0 MKOH	0-0.45V	2.03F cm <sup>-2</sup> 2.1mA cm <sup>-2</sup>	21
NiCo-LDH Ag /carbon cloth	1.0 MKOH	0-0.45V	1.1333F cm <sup>-2</sup> 1mA cm <sup>-2</sup>	22
NiCo-LDH nanosheets	1.0 MKOH	0-0.45V	6.37F/cm <sup>2</sup> (525 F/g) at 8 mA/cm <sup>2</sup>	23
carbon–CoO–NiO–NiCo <sub>2</sub> O <sub>4</sub> nanosheet	6.0 M KOH	0-0.48V	5.23 F/cm <sup>2</sup> (2602 F/g) at 2 mA/cm <sup>2</sup>	24
CoO@C nanostructure arrays	6.0 M KOH	-0.2-0.4V	6.76 F/cm <sup>2</sup> (3282.2 F/g) at 1 mA/cm <sup>2</sup>	25
Ni–Co LDH	1.0 M KOH	0-0.4V	9.98 F/cm <sup>2</sup> (2170 F/g) at 1 A/g	26
Polyaniline –Toray paper	Aqueous electrolyte	0-0.8V	1.3 F/cm <sup>2</sup> (1335 F/g) at 10 A/g	27
CoMoO <sub>4</sub> –MnO <sub>2</sub> core–shell nanosheet	1.0 M KOH	0-0.45V	8.01 F/cm <sup>2</sup> (2666.7F/g) at 3 mA/cm <sup>2</sup>	28
Ni <sub>3</sub> S <sub>2</sub> @Co(OH) <sub>2</sub> nano-wires /Ni Foam	3.0 MKOH	0-0.5V	13.5 F/cm <sup>2</sup> (2139.4 F/g) at 2 mA/cm <sup>2</sup>	29
Core–Shell NiMoO <sub>4</sub> @Ni–Co–S	2.0 M KOH	0-0.5V	2.27 F/cm <sup>2</sup> (1892 F/g) at 5 mA/cm <sup>2</sup>	30
CoMoO <sub>4</sub> @Co <sub>3</sub> O <sub>4</sub> /OMEP	2.0 M KOH	0-0.45V	7.13 F/cm <sup>2</sup> (1168 F/g) at 4 mA/cm <sup>2</sup>	31
CoMoO <sub>4</sub> @NiMoO <sub>4</sub> /Ni foam	2.0 M KOH	0-0.5V	3.33 F/cm <sup>2</sup> (1658.9 F/g) at 8 mA/cm <sup>2</sup>	32
NiCo <sub>2</sub> O <sub>4</sub> –MnMoO <sub>4</sub> /Ni foam	2.0 M KOH	0-0.5V	1.91 F/cm <sup>2</sup> (2010.5 F/g) at 1 mA/cm <sup>2</sup>	33
ZnCo <sub>2</sub> O <sub>4</sub> @MnO <sub>2</sub> /Ni foam	1.0 M KOH	0-0.5V	2.60 F/cm <sup>2</sup> (2170 F/g) at 3 mA/cm <sup>2</sup>	34
Cu <sub>1-x</sub> Nixs nanosheets	2.0 M KOH	0-0.5V	5.88 F/cm <sup>2</sup> (2672 F/g) at 2 mA/cm <sup>2</sup>	35
Ni/GF/H–CoMoO <sub>4</sub>	3.0 M KOH	0-0.5V	5.36 F/cm <sup>2</sup> (1472F/g) at 1mA/cm <sup>2</sup>	36
CoMoO <sub>4</sub> @MnO <sub>2</sub> /Ni foam	1.0 M KOH	0-0.5V	2.27 F/cm <sup>2</sup> (2159.4F/g) at 3 mA/cm <sup>2</sup>	37
NiCo <sub>2</sub> O <sub>4</sub> –MnO <sub>2</sub> /GF	6.0 M KOH	0-0.45V	5.16 F/cm <sup>2</sup> (2577F/g) at 2mA/cm <sup>2</sup>	38
NiCoP/Nickel Foam-Nanoarray	2.0 M KOH	0-0.5V	9.2 F cm <sup>-2</sup> 50mA cm <sup>-2</sup>	39
CF@NiPx Nanoflakes	6M KOH	0-0.4V	817 F cm <sup>-3</sup> 2 mA cm <sup>-2</sup>	40

## References:

- [1] C. An, Y. Wang, Y. Wang, G. Liu, L. Li, F. Qiu, Y. Xu, L. Jiao, H. Yuan, *RSC Adv.*, 2013, **3**, 4628-4633.
- [2] D. Wang, L. Kong, M. Liu, W. Zhang, Y. Luo, L. Kang, *Journal of Power Sources*, 2015, **274**, 1107-1113.

- [3] S. Duan, R. Wang, *NPG Asia Materials*, 2014, **6**, e00.
- [4] X. Chen, M. Cheng, D. Chen, R. Wang, *ACS Appl. Mater. Interfaces*, 2016, **8**, 3892-3900.
- [5] D. Wang, L. Kong, M. Liu, Y. Luo, L. Kang, *Chem. Eur. J.*, 2015, **21**, 17897-17903.
- [6] Y. Hu, M. Liu, Y. Hu, Q. Yang, L. Kong, L. Kang, *Electrochimica Acta*, 2016, **215**, 114-125.
- [7] S. Xie, J. Gou, *Journal of Alloys and Compounds*, 2017, **713**, 10-17.
- [8] Y. Shao, Y. Zhao, H. Li, C. Xu, *ACS Appl. Mater. Interfaces*, 2016, **8**, 35368-35376.
- [9] Y. Chen, Z. Chen, Y. Lin, Y. Hsu, *ACS Sustainable Chem. Eng.*, 2017, **5**, 3863-3870.
- [10] C. Wang, Y. Qian, J. Yang, S. Xing, X. Ding, Q. Yang, *RSC Adv.*, 2017, **7**, 26120-26124.
- [11] H. Liang, C. Xia, Q. Jiang, A. N. Gandi, U. Schwingenschlögl, H. N. Alshareef, *Nano Energy*, 2017, **35**, 331-340.
- [12] H. Wan, L. Li, Y. Chen, J. Gong, M. Duan, C. Liu, J. Zhang, Hao Wang, *Electrochimica Acta*, 2017, **229**, 380-386.
- [13] H. Wu, Y. Ni, M. Wang, D. Lu, *CrystEngComm*, 2016, **18**, 5155-5163.
- [14] X. Li, R. Ding, W. Shi, Q. Xu, L. Wang, H. Jiang, Z. Yang, E. Liu, *Materials Letters*, 2017, **187**, 144-147.
- [15] X. Li, R. Ding, L. Yi, W. Shi, Q. Xu, E. Liu, *Electrochimica Acta*, 2016, **222**, 1169-1175.
- [16] G. Zhang, J. Fang, L. Sun, S. Li, K. Xu, *Materials Science in Semiconductor Processing*, 2017, **66**, 140-143.
- [17] M. Kong, Z. Wang, W. Wang, M. Ma, D. Liu, S. Hao, R. Kong, G. Du, A. M. Asiri, Y. Yao, X. Sun, *Chem. Eur. J.*, 2017, **23**, 4435-4441.
- [18] Q. Chen, D. Cai, H. Zhan, *Journal of Alloys and Compounds*, 2017, **721**, 205-212.
- [19] D. Shi, L. Zhang, H. Gong, *Journal of Power Sources*, 2017, **361**, 9-14.
- [20] P. Venkateswarlu, E. Umeshbabu, U. N. Kumar, P. Nagaraja, P. Tirupathi, G. R. Rao, P. Justin, *Journal of Colloid and Interface Science*, 2017, **503**, 17-27.
- [21] T. Nguyen, M. Boudard, M. J. Carmezim, M. F. Montemor, *Energy*, 2017, **126**, 208-216.
- [22] S. C. Sekhar, G. Nagaraju, J. S. Yu, *Nano Energy*, 2017, **36**, 58-67.

- [23] L. Zhi, W. Zhang, L. Dang, J. Sun, F. Shi, H. Xu, Z. Liu, Z. Lei, *Journal of Power Sources*, 2018, **387**, 108-116.
- [24] H. Wang, J. Guo, C. Qing, D. Sun, B. Wang, Y. Tang, *Chem. Commun.*, 2014, **50**, 8697-8700.
- [25] H. Wang, C. Qing, J. Guo, A. A. Aref, D. Sun, B. Wang, Y. Tang, *J. Mater. Chem. A*, 2014, **2**, 11776-11783.
- [26] Y. Liu, X. Teng, Y. Mi, Z. Chen, *J. Mater. Chem. A*, 2017, **5**, 24407-24415.
- [27] R. Soni, V. Kashyap, D. Nagaraju, S. Kurungot, *ACS Appl. Mater. Interfaces*, 2018, **10**, 676-686.
- [28] S. Kumar, G. Saeed, N. H. Kim, J. H. Lee, *J. Mater. Chem. A*, 2018, **6**, 7182-7193.
- [29] F. Chen, H. Wang, S. Ji, V. Linkov, R. Wang, *Chemical Engineering Journal*, 2018, **345**, 48-57.
- [30] C. Chen, D. Yan, X. Luo, W. Gao, G. Huang, Z. Han, Y. Zeng, Z. Zhu, *ACS Appl. Mater. Interfaces*, 2018, **10**, 4662-4671.
- [31] M. Li, Y. Wang, H. Yang and P. K. Chu, *J. Mater. Chem. A*, 2017, **5**, 17312-17324.
- [32] Z. Zhang, H. Zhang, X. Zhang, D. Yu, Y. Ji, Q. Sun, Y. Wang, X. Liu, *J. Mater. Chem. A*, 2016, **4**, 18578-18584.
- [33] C. Cui, J. Xu, L. Wang, D. Guo, M. Mao, J. Ma, T. Wang, *ACS Appl. Mater. Interfaces*, 2016, **8**, 8568-8575.
- [34] D. Yu, Z. Zhang, Y. Meng, Y. Teng, Y. Wu, X. Zhang, Q. Sun, W. Tong, X. Zhao, X. Liu, *Inorg. Chem. Front.*, 2018, **5**, 597-604.
- [35] J. Balamurugan, C. Li, T. D. Thanh, O. Park, N. H. Kim, J. H. Lee, *J. Mater. Chem. A*, 2017, **5**, 19760-19772.
- [36] K. Chi, Z. Zhang, Q. Lv, C. Xie, J. Xiao, F. Xiao, S. Wang, *ACS Appl. Mater. Interfaces*, 2017, **9**, 6044-5053.
- [37] Z. Zhang, F. Bao, Y. Zhang, L. Feng, Y. Ji, H. Zhang, Q. Sun, S. Feng, X. Zhao, X. Liu, *J. Power Sources*, 2015, **296**, 162-168.
- [38] M. A. Garakani, S. Abouali, Z. Xu, J. Huang, J. Huang, J. Kim, *J. Mater. Chem. A*, 2017, **5**, 3547-3557.

- [39] M. Kong, Zao Wang, W. Wang, M. Ma, D. Liu, S. Hao, R. Kong, G. Du, A. M. Asiri, Y. Yao, X. Sun, *Chem. Eur. J.*, 2017, **23**, 4435-4441.
- [40] Z. Zhang, S. Liu, J. Xiao, S. Wang, *J. Mater. Chem. A*, 2016, **4**, 9691-9699.